Monolayer Molecular Functionalization Enabled by Acid-Base Interaction for High-Performance Photochemical CO_2 Reduction

Bo Shang,[a,b] Fengyi Zhao,[c] Chungseok Choi,[a,b] Xiaofan Jia,[a] Magnus Pauly,[d] Yueshen Wu,[a,b] Zixu Tao,[a,b] Yiren Zhong,[a,b] Nia Harmon,[a,b] Paul A. Maggard,[d] Tianquan Lian,[c] Nilay Hazari,[a] and Hailiang Wang*[a,b]

a. Department of Chemistry, Yale University, New Haven, Connecticut, 06520, USA

Email: hailiang.wang@yale.edu

b. Energy Sciences Institute, Yale University, West Haven, Connecticut, 06516, USA

c. Department of Chemistry, Emory University, 1515 Dickey Drive, Atlanta, Georgia, 30322, United States

d. Department of Chemistry, North Carolina State University, Raleigh, North Carolina, 27695-8204, United States

ABSTRACT

We report the development of a hybrid catalyst consisting of carbon nitride (CN_x) and cobalt phthalocyanine tetracarboxylic acid (CoPc-COOH), which converts CO_2 to CO with high reaction rate (1067 μmol/g·h) and high selectivity (over 98%), under simulated solar irradiation. The carboxylic acid substituents on the phthalocyanine ligands play a critical role as they bind to the amine groups of CN_x to enable nearly ideal monolayer coverage of the molecular co-catalyst on the semiconductor surface and promote catalytic activity from the molecular complex. Specifically, the CN_x/CoPc-COOH hybrid material achieves a reaction rate 16 times higher than a CN_x material containing unsubstituted CoPc molecules. We further show that activation and deactivation of the CN_x/CoPc-COOH composite, which are associated with the reduction and decomposition of CoPc-COOH, respectively, both proceed at a nearly constant rate regardless of the CO_2 reduction reaction rate. The decoupling of charge carrier injection and CO_2 reduction catalysis has important mechanistic implications for future performance optimization and materials design of photocatalysts for CO_2 reduction.

The rising concentration of CO_2 in the atmosphere and the depletion of our fossil fuel reserves make it desirable to produce fuels and commodity chemicals using CO_2 as a feedstock.[1-3] Photoreduction is one of the most direct methods to harvest sunlight and valorize CO_2[4-8] and numerous semiconductor materials have been explored as photocatalysts for CO_2 reduction.[9-17] Among them, carbon nitride (CN_x) based materials possess significant advantages because they are inexpensive, easy to produce on large scale, and do not contain any noble or toxic metals.[18-22] However, in catalytic systems for CO_2 reduction involving CN_x, a co-catalyst is often required to give high rates and selectivity. For example, Li et al. developed a CN_x catalyst containing single-atom cobalt sites, which achieved a turnover number (TON) >200 for CO_2 reduction to CO, with a selectivity of approximately 80%.[23] Given the well-defined structures and tunability of molecular transition-metal catalysts, it would be desirable to use them to both improve performance and elucidate mechanistic pathways,[24-26] but at this stage it is challenging to achieve high and uniform coverage of molecular catalysts on CN_x surfaces.

Cobalt phthalocyanine (CoPc) is one of the most widely studied and best performing molecular catalysts for CO_2 electroreduction.[27] Its catalytic performance can be enhanced by both hybridization with carbon nanotubes and tuning of the electronic properties of the Pc ligand to enable more efficient production of CO or generation of liquid products such as methanol.[28-32] However, there has been only a limited number of studies exploring CoPc as a catalyst for photochemical CO_2 reduction. Additionally, previous studies commonly use CoPc as a light absorber but not a co-catalyst.[33-36] Recently, Ouyang et al. constructed a molecular assembly of a CoPc co-catalyst and a pyridine-appended iridium photosensitizer, which gave quantum yields of up to 27.9% for CO_2 reduction to CO but relies on noble metal materials.[37] Similar molecular structures such as Co quaterpyridine complexes and polymeric CoPc have been loaded onto CN_x to generate systems for CO_2 photoreduction.[14, 38-39] Nevertheless, the reaction rate and/or turnover frequency (TOF) remain relatively low. Our prior research has shown that high catalytic performance can be enabled by high coverage and uniform distribution of individual catalyst molecules on support materials.[24, 28-29]

Therefore, it is important to formulate specific molecule-material interactions for achieving mono-dispersion of co-catalyst molecules, which will not only enhance the photocatalytic performance, but also provide a well-defined system for studying interfacial charge transfer, molecular catalysis, and activation/deactivation to answer important mechanistic questions. For example, it is known that CoPc molecules need to be reduced before they can transfer electrons to CO_2; however, the reduction state of the real active catalyst remains elusive.[29, 40] Furthermore, CoPc-based photocatalysts are known to deactivate under UV illumination,[41] but the mechanism has not been investigated in detail.

In this work, we achieve nearly monolayer coverage of cobalt phthalocyanine tetracarboxylic acid (CoPc-COOH) molecules on CN_x by taking advantage of the acid-base interaction between the amine groups on the CN_x and the carboxyl groups of CoPc-COOH. The resulting CN_x/CoPc-COOH hybrid material shows a high photocatalytic activity of 1067 $\mu mol \cdot g^{-1} \cdot h^{-1}$ with selectivity of over 98% for CO_2 reduction to CO under illumination from an AM1.5G-filtered 150 W Xe lamp (300 mW/cm^2). This is higher than most previously supported systems for CO_2 reduction based on CN_x semiconductors. We show that the -COOH groups are responsible for both the strong interaction with the CN_x substrate and the high catalytic activity of the CoPc-COOH molecules. For example, CN_x/CoPc-COOH gives 8 times higher co-catalyst loading and 16 times higher reaction rate compared to a control material with unsubstituted CoPc (CN_x/CoPc). We also studied the activation and deactivation of the CN_x/CoPc-COOH hybrid. The activation is associated with multiple-electron reduction of the supported CoPc-COOH molecules by photoelectrons, whereas the deactivation is caused by CoPc-COOH decomposition and leaching of the metal into the solution. Intriguingly, the activation and deactivation rates are independent of the photocatalytic activity or substituents on the CoPc structure, which indicates that electron injection into the molecular co-catalyst and subsequent CO_2 reduction catalysis may be decoupled in this system, providing a new strategy for photocatalyst design and optimization.

CN_x was made via pyrolysis of urea according to a literature method (**Figure S1**).[21] CoPc-COOH molecules were then assembled onto the CN_x surface (input CoPc-COOH:CN_x ratio = 5 wt.%) by ultrasonication of CN_x in a *N*,*N*-dimethylformamide (DMF) solution of CoPc-COOH (**Figure 1**a, see Supporting Information, SI 1.c for experimental details). The color of CN_x changes from light yellow to cyan blue after the loading of CoPc-COOH (**Figure S2**). Scanning electron microscopy (SEM) shows the nanosheet microstructure of the CN_x/CoPc-COOH hybrid material (**Figure 1**b). Aberration-corrected scanning transmission electron microscopy (AC-STEM), which shows atomic-number-dependent contrast, suggests dense and relatively uniform distribution of Co atoms on CN_x (**Figure 1**c). Energy-dispersive X-ray spectroscopy (EDS) mapping confirms the uniform distribution of CoPc-COOH molecules on the CN_x surface (**Figure 1**d and S3).

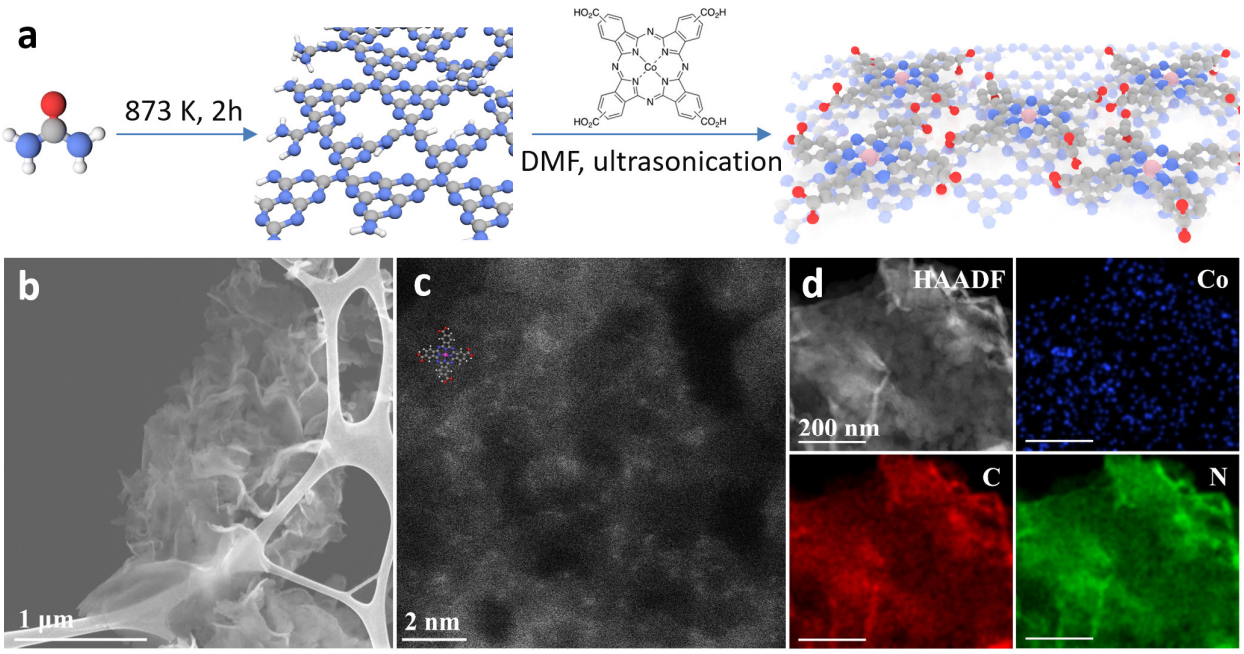

Figure 1. (a) Schematic illustration of CN_x/CoPc-COOH preparation. (b) SEM image of CN_x/CoPc-COOH on a lacey carbon film support. (c) AC-STEM image of CN_x/CoPc-COOH. The inset shows a CoPc-COOH molecule drawn to scale. (d) EDS mapping of Co, C, and N elements in CN_x/CoPc-COOH.

The mass loading of CoPc-COOH in the hybrid material was quantified by inductively coupled plasma mass spectrometry (ICP-MS) to be 2.4 wt.%. Interestingly, this value matches our calculated maximum loading for CoPc-COOH monolayer coverage on CN_x (see SI 2.d for details). As the input amount ratio of CoPc-COOH to CN_x is lowered, the loading decreases linearly (**Figure 2**a). However, no obvious increase in loading is observed when the input amount is increased to 10 wt.%, which confirms that the CN_x surface has indeed been saturated at the 2.4 wt.% loading. The efficiency of assembling CoPc-based molecules onto CN_x surfaces is strongly dependent on the structure of the molecule and the type of CN_x. Unsubstituted CoPc and perfluorinated CoPc (CoPc-F) (**Figure S4**) show 8 and 12 times lower loadings than CoPc-COOH under identical assembly conditions (**Figure 2**a), respectively. This result indicates that the -COOH groups may play an important role in binding the CN_x surface. When melamine is replaced for urea as the precursor, the resulting CN_x (m-CN_x) is much less effective in binding CoPc-COOH. The same assembly conditions lead to a 4 times lower loading (**Figure 2**a). FTIR characterization was performed for CN_x and m-CN_x. The spectra (**Figure 2**b) were normalized by the C-N stretching peak at 1226 cm^{-1} considering that these materials should have roughly comparable numbers of C-N bonds. The results reveal that m-CN_x has more heptazine but less N-H moieties than (urea-derived) CN_x (**Figure 2**b), indicating a higher density of surface -NH_2 groups and a lower degree of polymerization for CN_x.[42] These results led us to hypothesize that the strong binding between CoPc-COOH and CN_x is because of the acid-base interaction between the -COOH and -NH_2 groups. While previous work has shown that hydrogen bonding can also enable supermolecular assembly,[43] it is unlikely to be the case here since CoPc-F does not bind strongly to CN_x.

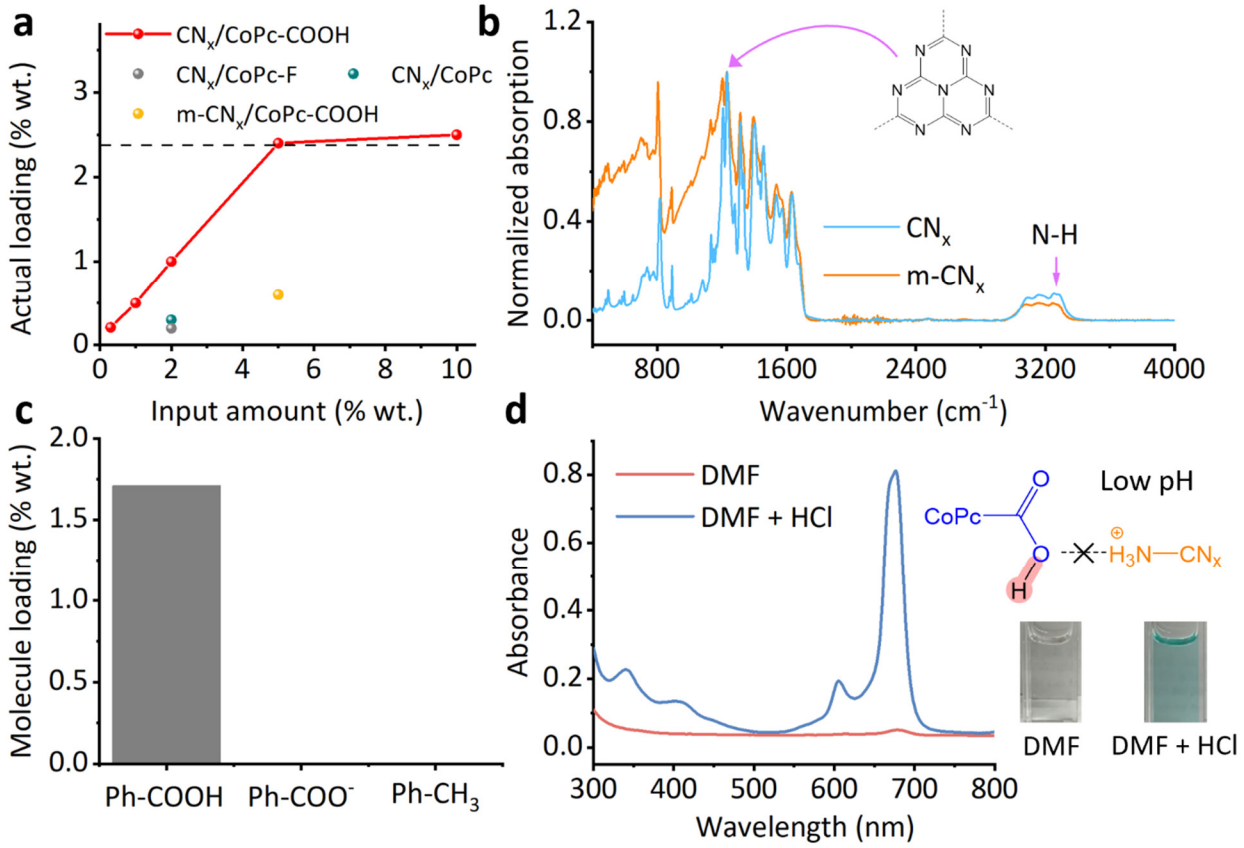

Figure 2. Acid-base interaction between CoPc-COOH and CN_x. (a) Correlation between actual loading and input amount for CoPc with different substituents assembled onto CN_x or m-CN_x. The black dashed line represents the estimated maximum loading for monolayer coverage of CoPc-COOH on CN_x. (b) FTIR spectra of CN_x and m-CN_x, with the heptazine and amine peaks labelled. (c) Loading of substituted benzene with different functional groups onto CN_x. (d) UV-vis spectra of solutions obtained from washing CN_x/CoPc-COOH with DMF or DMF + HCl. Inset shows photos of the solutions.

To test this hypothesis, we studied the assembly between benzoic acid and CN_x (SI 1.d). We find that benzoic acid molecules can be effectively loaded onto CN_x, readily reaching a mass loading of 1.7% (**Figure 2**c and S5). In contrast, toluene can barely be loaded onto CN_x, consistent with the -COOH group playing a significant role. Notably, when benzoic acid is basified to form benzoate, assembly with CN_x does not happen, which suggests that it is the acidic character of the -COOH group that is responsible for

the strong interaction with CN_x. Returning to the CN_x/CoPc-COOH hybrid, the loaded CoPc-COOH molecules cannot be removed from the CN_x by washing with DMF (**Figure 2**d and SI 1.e). However, if a mixed solution of DMF and HCl is used (SI 1.e), a substantial amount of CoPc-COOH is washed away, presumably because the HCl protonates the CoPc-COO^- on the CN_x surface and disrupts the acid-base interaction (**Figure 2**d). Together, these results support that the CoPc-COOH assembly with CN_x is driven by the acid-base interaction between the -COOH and -NH_2 groups.

The CN_x/CoPc-COOH hybrid material (2.4 wt.% co-catalyst loading unless otherwise stated) was investigated for photocatalytic CO_2 reduction under illumination from an AM1.5G-filtered 150W Xe lamp (300 mW/cm^2, 3 cm^2) with triethanolamine (TEOA) as the electron donor and acetonitrile as the solvent. It takes 1 h for the photocatalyst to be activated and reach the maximum CO_2 reduction rate of 1067 $\mu mol \cdot g^{-1} \cdot h^{-1}$ (normalized to the total mass of CN_x/CoPc-COOH, **Figure 3**a), corresponding to a TOF of 33.2 h^{-1} (normalized to the total number of CoPc-COOH molecules, **Figure S6**). After the rate peaks, the performance starts to decay gradually, giving a value of 780 $\mu mol \cdot g^{-1} \cdot h^{-1}$ after 8 h. CO is produced with a selectivity of over 98% (H_2 is the other reduction product) throughout the reaction period (**Figure 3**a), and the TON is 221. When the reaction is illuminated with a 365 nm LED light, an apparent quantum yield of 0.90% is measured (SI 2.b). Our CN_x/CoPc-COOH outperforms almost all CN_x-based photocatalysts reported to date under comparable conditions (**Figure 3**b and Table S1).[14, 23, 38, 44-51] Without CoPc-COOH, CN_x alone shows essentially no activity for CO_2 reduction (Table S2), corroborating the critical role of the molecular co-catalyst. As we decrease the CoPc-COOH loading gradually from 2.4 wt.% to 0.2 wt.%, the reaction rate decreases whereas the TOF increases (**Figure 3**c, S6), which is a common phenomenon in catalysis as the number of catalytic sites decreases.[52-53] However, when we further increase the loading beyond 2.4 wt.%, which is the monolayer coverage limit, the reaction rate starts to decrease (**Figure 3**c). In particular, a physical mixture of CN_x containing 10 wt.% of CoPc-COOH shows no activity. This indicates that the dispersion of the molecular catalyst is critical for the reaction. It is likely that aggregated

CoPc-COOH, which is electrically insulating, cannot efficiently transfer electrons from the CN_x to CO_2, as we have demonstrated earlier for electrocatalysis.[24, 29]

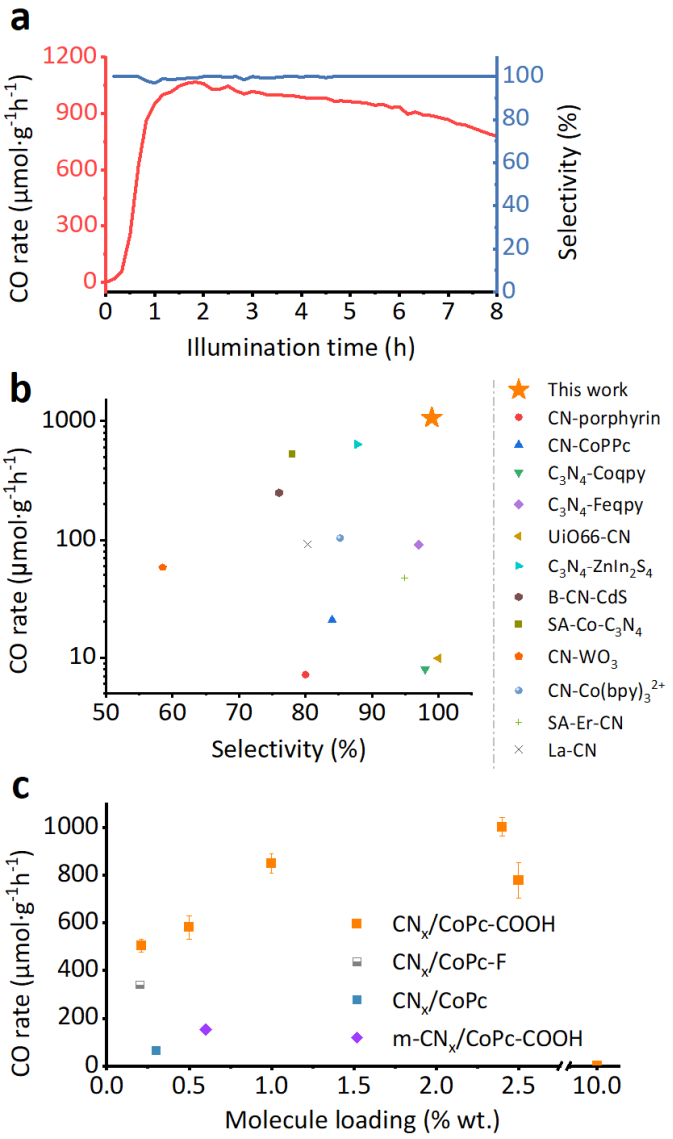

Figure 3. (a) Reaction rate and selectivity of photochemical CO_2 reduction to CO catalyzed by CN_x/CoPc-COOH. (b) Comparison of photocatalytic performance with other CN_x-based photocatalyst materials reported in the literature (see Table S1 for details). (c) Loading-dependent CO production rate of CoPc with different substituents supported on CN_x or m-CN_x.

We find the photocatalytic performance is highly dependent on the CoPc substituent and the type of CN_x. CN_x functionalized with CoPc-F and unsubstituted CoPc respectively show 1.5 and 8.0 times lower reaction rates and 1.8 and 15 times lower TOFs than CN_x/CoPc-COOH at comparable loadings (**Figure 3**c, S6). This result is indicative of the critical role of the -COOH groups in rendering the high performance of the CN_x/CoPc-COOH photocatalyst. Replacing CN_x with m-CN_x or a crystalline CN_x[54] (**Figure S7**, SI 1.f) also significantly lowers the photocatalytic reaction rate (**Figure 3**c, Table S2), suggesting that the exact structure of the CN_x light absorber also plays a crucial role in the photochemical CO_2 reduction reaction, likely by impacting the charge carrier generation, separation, and transfer processes.

The CN_x/CoPc-COOH photocatalyst exhibits obvious activation and deactivation behavior (**Figure 4**a, S8), which is often observed in other photochemical CO_2 reduction studies but is not well understood.[14, 37] We first studied the activation process. We observe that the color of the CN_x/CoPc-COOH photocatalyst changes from cyan to white 15 min after the CO_2 photoreduction reaction starts (**Figure S9**a). In-situ UV-vis measurements were performed to characterize the process (**Figure 4**b). The starting CN_x/CoPc-COOH suspension shows a characteristic absorption peak at 696 nm, which quickly diminishes after 3 mins of illumination. Meanwhile, the 732 nm peak rises. As the illumination continues, the 732 nm peak gradually decreases in intensity. We hypothesize these color and spectral changes are associated with the reduction of CoPc-COOH. Indeed, the original cyan color can be quickly restored when the activated/reduced photocatalyst is re-exposed to air (**Figure S9**b). An identical phenomenon is observed in Ar atmosphere (**Figure S9**c), suggesting that CO_2 is not involved in the CoPc-COOH pre-reduction process. X-ray photoelectron spectroscopy (XPS) measurement of the fully activated CN_x/CoPc-COOH reveals a shift of 0.65 eV to lower binding energy for the Co 2p electrons compared to the initial CN_x/CoPc-COOH (**Figure 4**c). Based on the direction and magnitude of this shift, we believe the Co center is reduced from +2 to +1 oxidation state in the activation process, which generates the real co-catalyst that enables CO_2 reduction to CO.

To further probe the reduction-based activation, we carried out chemical reduction of CoPc-COOH in its DMF solution by KC_8 and monitored the reduction process with UV-vis spectroscopy (SI section 1.g). The starting CoPc-COOH solution shows a main absorption feature at 665 nm, which has the same origin as the 696 nm absorption of the CN_x/CoPc-COOH suspension. The peak shift is likely caused by interaction with CN_x. Upon stepwise reduction, the CoPc-COOH solution changes from the original cyan color to light green, light yellow, and then light pink (**Figure S**10). Comparing the absorption spectra with the aforementioned in-situ results shows that two-electron reduced CoPc-COOH is formed after about 3 min of activation under the photochemical reaction conditions, whereas 40 min of illumination yields four-electron reduced CoPc-COOH. Considering that the CN_x/CoPc-COOH catalyst experiences an incubation time (the first activation period where the activity is near zero) of about 20 mins and takes about 1 h of total activation time to reach its peak performance (**Figure 3**a), we propose that the four-electron reduced CoPc-COOH is the main species active for reducing CO_2, and that the one- or two-electron reduced CoPc-COOH has no CO_2 reduction activity. We also find the two-electron reduced CoPc-COOH from the chemical reduction can be easily re-oxidized by air (**Figure S**11), consistent with the behavior of the CN_x/CoPc-COOH photocatalyst (**Figure S9**b). The fact that the color restoration cannot occur in CO_2 atmosphere confirms that the two-electron reduced CoPc-COOH is not active for CO_2 reduction. To the best of our knowledge, this is the first time that the reduction state of active CoPc species for CO_2 reduction is identified.

Transient absorption measurements of CN_x/CoPc-COOH were carried out to study the dissipation kinetics of photogenerated electrons (SI 2.g). The results show a faster decay after the photocatalyst material is activated (**Figure 4**d and S12), suggesting that the activation also improves the charge transfer between CN_x and the CoPc-COOH molecules.[17, 55-56] As we vary the loading of CoPc-COOH, we find a clear linear relationship between activation time and loading (**Figure 4**e). This again confirms that the activation process is the reduction of CoPc-COOH which seems to proceed at a constant rate (i.e., roughly the same

number of CoPc-COOH molecules are activated per unit time) in this case. Interestingly, CN_x/CoPc and CN_x/CoPc-F fit the line well despite their much lower photocatalytic activity than CN_x/CoPc-COOH, which indicates that the activation is neither affected by substituents on CoPc nor directly associated with the CO_2 reduction process.

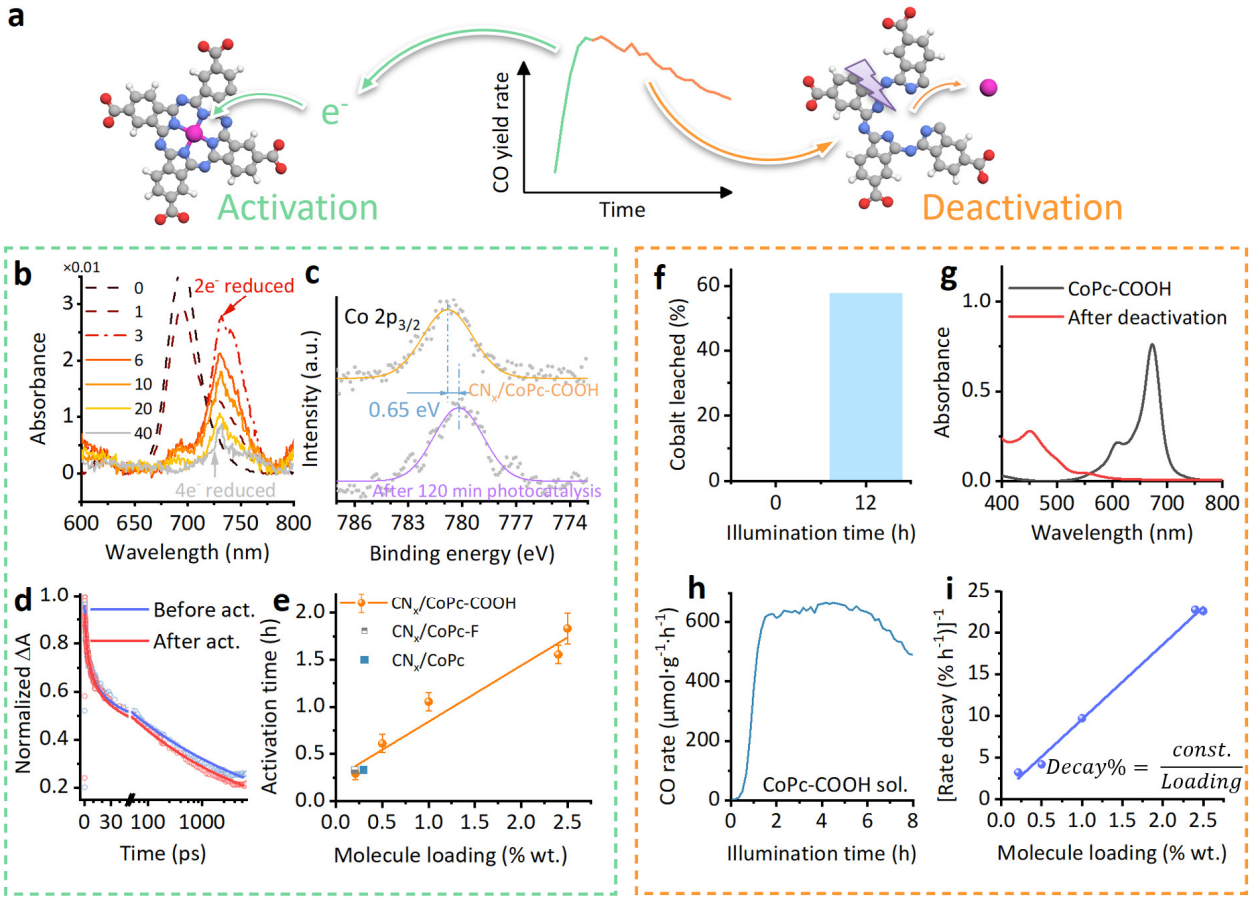

Figure 4. (a) Hypothetical activation and deactivation mechanisms of CoPc-COOH. (b) In-situ UV-vis spectra of CN_x/CoPc-COOH with varied illumination time (in min). (c) Co $2p_{3/2}$ XPS spectra of CN_x/CoPc-COOH before and after activation. (d) Normalized transient absorption kinetics of a CN_x/CoPc-COOH film before and after activation. The dots represent the original data points, and the lines represent the fitted power-law decay curves. (e) Correlation between activation time and co-catalyst loading. (f) Percentage of Co detected in the solution before and after reaction. (g) UV-vis spectrum of the filtered reaction solution after deactivation, in comparison with CoPc-COOH dissolved in the same mixed solvent (acetonitrile/TEOA). (h) Photocatalytic CO_2

reduction performance of CN_x with CoPc-COOH (dissolved in DMF) added to the acetonitrile/TEOA reaction solution. (i) Correlation between reciprocal deactivation rate and CoPc-COOH loading.

We then analyzed the deactivation process. After 12 h of photochemical CO_2 reduction (**Figure S13**), we find using ICP-MS that 58% of the Co in the starting CN_x/CoPc-COOH has leached into the solution (**Figure 4**f). UV-vis inspection of the post-reaction solution shows no absorption features that belong to pristine or reduced CoPc-COOH (**Figure 4g**, S10), indicating that the leached Co is not coordinated by the Pc ligand anymore. Indeed, if we run the CO_2 reduction reaction using CN_x as the photocatalyst with the CoPc-COOH co-catalyst (2.4 wt.% of CN_x) dissolved in the solution (DMF was included in the solution to enable CoPc-COOH dissolution, SI 2.a), a reasonably high CO production rate can still be realized (**Figure 4**h), which confirms that the deactivation of CN_x/CoPc-COOH is not due to simple dissolution of the co-catalyst molecules into the solution but is caused by permanent decomposition of CoPc-COOH. On this basis, we can derive the following equation for the relative deactivation rate if we assume each active CoPc-COOH molecule makes equal contribution to the reaction activity:

$$\text{Deactivation rate} = \frac{\text{Number of CoPc—COOH molecules deactivated per hour}}{\text{Total number of CoPc—COOH molecules (Loading)}}$$

The deactivation rate here is defined as the percentage decrease of the reaction rate (per hour) and is determined from fitting the linear region after the peak reaction rate on the rate vs time curve (**Figure S**14). Plotting the reciprocal deactivation rate vs CoPc-COOH loading yields a straight line (**Figure 4**i), suggesting that the number of CoPc-COOH molecules that are deactivated per hour is a constant regardless of the overall reaction rate or TOF for CO_2 reduction (Table S3). Although the actual cause of CoPc-COOH decomposition is not clear at this stage, it is likely not directly associated with the CO_2 reduction process. Despite the deactivation, our CN_x/CoPc-COOH catalyst is able to yield a total CO amount of 26.8 mmol per gram of catalyst, which is one of the best among CN_x-based photocatalysts (Table S1).

The observation that both activation and deactivation proceed at constant rates independent of the CO_2 reduction performance indicates that these two processes likely do not directly involve CO_2. We therefore propose that they are driven by charge carriers injected from the CN_x light absorber. Considering that the activation rate is independent of the presence or type of substituents on CoPc (**Figure 4**e), we infer photoelectrons are transferred from CN_x to the co-catalyst molecules through the π plane rather than the functional group. On the other hand, the CO_2 reduction rate has a strong dependence on CoPc substituents (**Figure 3**c), which indicates that it may be controlled by the electron transfer from the co-catalyst to CO_2. Hence, we conclude that the CO_2 reduction catalysis on the co-catalyst molecule is decoupled from the charge injection at the CN_x/co-catalyst interface. This implies the possibility to improve the reaction system by optimizing these two steps separately. Taken together, the -COOH substituents play two major roles in this reaction system: i) they enable effective loading of co-catalyst molecules on the light absorber via acid-base interaction; ii) they improve the catalytic activity of CoPc for CO_2 reduction to CO.

In summary, we have successfully developed an acid-base interaction strategy for assembling CoPc-COOH molecular co-catalysts onto CN_x surfaces with nearly monolayer coverage. The resulting CN_x/CoPc-COOH photocatalyst shows high CO_2 reduction performance and is one of most active CN_x based systems reported to date. Additionally, via our study of the activation and deactivation mechanisms, we have provided molecular-level insight into the photocatalytic CO_2 reduction reaction, which may be valuable for the design of improved systems.

Supporting Information

Experimental details, additional characterization results, molecular structures, additional analysis results, and catalytic performance comparison (PDF)

Acknowledgments

This work was solely supported as part of the Center for Hybrid Approaches in Solar Energy to Liquid Fuels (CHASE), an Energy Innovation Hub funded by the U.S. Department of Energy, Office of Science, Office of Basic Energy Sciences under Award Number DE-SC0021173. The Xe lamp used in this work was purchased with internal funding from the Center for Research on Interface Structures and Phenomena at Yale University.

References

1. Solomon, S.; Plattner, G.-K.; Knutti, R.; Friedlingstein, P., Irreversible climate change due to carbon dioxide emissions. *Proceedings of the national academy of sciences* **2009,** *106* (6), 1704-1709.
2. Kondratenko, E. V.; Mul, G.; Baltrusaitis, J.; Larrazábal, G. O.; Pérez-Ramírez, J., Status and perspectives of CO_2 conversion into fuels and chemicals by catalytic, photocatalytic and electrocatalytic processes. *Energy & environmental science* **2013,** *6* (11), 3112-3135.
3. Ross, M. B.; De Luna, P.; Li, Y.; Dinh, C.-T.; Kim, D.; Yang, P.; Sargent, E. H., Designing materials for electrochemical carbon dioxide recycling. *Nature Catalysis* **2019,** *2* (8), 648-658.
4. Li, X.; Yu, J.; Jaroniec, M.; Chen, X., Cocatalysts for Selective Photoreduction of CO_2 into Solar Fuels. *Chemical Reviews* **2019,** *119* (6), 3962-4179.
5. Li, K.; Teng, C.; Wang, S.; Min, Q. H., Recent Advances in TiO_2-Based Heterojunctions for Photocatalytic CO_2 Reduction With Water Oxidation: A Review. *Front Chem* **2021,** *9*, 637501.
6. Albero, J.; Peng, Y.; Garcia, H., Photocatalytic CO_2 Reduction to C_2+Products. *Acs Catalysis* **2020,** *10* (10), 5734-5749.
7. Takata, T.; Jiang, J.; Sakata, Y.; Nakabayashi, M.; Shibata, N.; Nandal, V.; Seki, K.; Hisatomi, T.; Domen, K., Photocatalytic water splitting with a quantum efficiency of almost unity. *Nature* **2020,** *581* (7809), 411-414.
8. Li, K.; Peng, B.; Peng, T., Recent Advances in Heterogeneous Photocatalytic CO_2 Conversion to Solar Fuels. *ACS Catalysis* **2016,** *6* (11), 7485-7527.
9. Jiang, Z.; Xu, X. H.; Ma, Y. H.; Cho, H. S.; Ding, D.; Wang, C.; Wu, J.; Oleynikov, P.; Jia, M.; Cheng, J.; Zhou, Y.; Terasaki, O.; Peng, T. Y.; Zan, L.; Deng, H. X., Filling metal-organic framework mesopores with TiO_2 for CO_2 photoreduction. *Nature* **2020,** *586*, 549.
10. Li, X. D.; Sun, Y. F.; Xu, J. Q.; Shao, Y. J.; Wu, J.; Xu, X. L.; Pan, Y.; Ju, H. X.; Zhu, J. F.; Xie, Y., Selective visible-light-driven photocatalytic CO_2 reduction to CH_4 mediated by atomically thin $CuIn_5S_8$ layers. *Nature Energy* **2019,** *4* (8), 690-699.
11. Yang, K. H.; Yang, Z. Z.; Zhang, C.; Gu, Y. L.; Wei, J. J.; Li, Z. H.; Ma, C.; Yang, X.; Song, K. X.; Li, Y. M.; Fang, Q. Z.; Zhou, J. W., Recent advances in CdS-based photocatalysts for CO_2 photocatalytic conversion. *Chem Eng J* **2021,** *418*, 129344.
12. Wu, Y. A.; McNulty, I.; Liu, C.; Lau, K. C.; Liu, Q.; Paulikas, A. P.; Sun, C.-J.; Cai, Z.; Guest, J. R.; Ren, Y.; Stamenkovic, V.; Curtiss, L. A.; Liu, Y.; Rajh, T., Facet-dependent active sites of a single Cu_2O particle photocatalyst for CO_2 reduction to methanol. *Nature Energy* **2019,** *4* (11), 957-968.
13. Yang, L.; Peng, Y.; Luo, X.; Dan, Y.; Ye, J.; Zhou, Y.; Zou, Z., Beyond C_3N_4 π-conjugated metal-free polymeric semiconductors for photocatalytic chemical transformations. *Chemical Society Reviews* **2021,** *50* (3), 2147-2172.
14. Roy, S.; Reisner, E., Visible-Light-Driven CO_2 Reduction by Mesoporous Carbon Nitride Modified with Polymeric Cobalt Phthalocyanine. *Angewandte Chemie International Edition* **2019,** *58* (35), 12180-12184.

15. Wang, S.; Teramura, K.; Hisatomi, T.; Domen, K.; Asakura, H.; Hosokawa, S.; Tanaka, T., Effective Driving of Ag-Loaded and Al-Doped $SrTiO_3$ under Irradiation at $\lambda > 300$ nm for the Photocatalytic Conversion of CO_2 by H_2O. *Acs Appl Energ Mater* **2020,** *3* (2), 1468-1475.
16. Kuehnel, M. F.; Orchard, K. L.; Dalle, K. E.; Reisner, E., Selective Photocatalytic CO_2 Reduction in Water through Anchoring of a Molecular Ni Catalyst on CdS Nanocrystals. *Journal of the American Chemical Society* **2017,** *139* (21), 7217-7223.
17. Yang, W.; Godin, R.; Kasap, H.; Moss, B.; Dong, Y.; Hillman, S. A. J.; Steier, L.; Reisner, E.; Durrant, J. R., Electron Accumulation Induces Efficiency Bottleneck for Hydrogen Production in Carbon Nitride Photocatalysts. *Journal of the American Chemical Society* **2019,** *141* (28), 11219-11229.
18. Zhou, Z.; Zhang, Y.; Shen, Y.; Liu, S.; Zhang, Y., Molecular engineering of polymeric carbon nitride: advancing applications from photocatalysis to biosensing and more. *Chemical Society Reviews* **2018,** *47* (7), 2298-2321.
19. Li, Y.; Li, B.; Zhang, D.; Cheng, L.; Xiang, Q., Crystalline Carbon Nitride Supported Copper Single Atoms for Photocatalytic CO_2 Reduction with Nearly 100% CO Selectivity. *ACS Nano* **2020,** *14* (8), 10552-10561.
20. Zhao, D.; Wang, Y.; Dong, C.-L.; Huang, Y.-C.; Chen, J.; Xue, F.; Shen, S.; Guo, L., Boron-doped nitrogen-deficient carbon nitride-based Z-scheme heterostructures for photocatalytic overall water splitting. *Nature Energy* **2021,** *6* (4), 388-397.
21. Liu, J.; Zhang, T.; Wang, Z.; Dawson, G.; Chen, W., Simple pyrolysis of urea into graphitic carbon nitride with recyclable adsorption and photocatalytic activity. *Journal of Materials Chemistry* **2011,** *21* (38), 14398-14401.
22. Zhang, Y.; Liu, J.; Wu, G.; Chen, W., Porous graphitic carbon nitride synthesized via direct polymerization of urea for efficient sunlight-driven photocatalytic hydrogen production. *Nanoscale* **2012,** *4* (17), 5300-5303.
23. Huang, P.; Huang, J.; Pantovich, S. A.; Carl, A. D.; Fenton, T. G.; Caputo, C. A.; Grimm, R. L.; Frenkel, A. I.; Li, G., Selective CO_2 Reduction Catalyzed by Single Cobalt Sites on Carbon Nitride under Visible-Light Irradiation. *Journal of the American Chemical Society* **2018,** *140* (47), 16042-16047.
24. Wu, Y.; Liang, Y.; Wang, H., Heterogeneous Molecular Catalysts of Metal Phthalocyanines for Electrochemical CO_2 Reduction Reactions. *Accounts of Chemical Research* **2021,** *54* (16), 3149-3159.
25. Ge, A.; Rudshteyn, B.; Videla, P. E.; Miller, C. J.; Kubiak, C. P.; Batista, V. S.; Lian, T., Heterogenized Molecular Catalysts: Vibrational Sum-Frequency Spectroscopic, Electrochemical, and Theoretical Investigations. *Accounts of Chemical Research* **2019,** *52* (5), 1289-1300.
26. Wang, J.; Dou, S.; Wang, X., Structural tuning of heterogeneous molecular catalysts for electrochemical energy conversion. *Science Advances* **2021,** *7* (13), eabf3989.
27. Yang, S.; Yu, Y.; Gao, X.; Zhang, Z.; Wang, F., Recent advances in electrocatalysis with phthalocyanines. *Chemical Society Reviews* **2021,** *50*, 12985-13011.
28. Wu, Y.; Jiang, Z.; Lu, X.; Liang, Y.; Wang, H., Domino electroreduction of CO_2 to methanol on a molecular catalyst. *Nature* **2019,** *575* (7784), 639-642.
29. Zhang, X.; Wu, Z.; Zhang, X.; Li, L.; Li, Y.; Xu, H.; Li, X.; Yu, X.; Zhang, Z.; Liang, Y.; Wang, H., Highly selective and active CO_2 reduction electrocatalysts based on cobalt phthalocyanine/carbon nanotube hybrid structures. *Nat Commun* **2017,** *8* (1), 1-8.
30. Choi, J.; Wagner, P.; Gambhir, S.; Jalili, R.; MacFarlane, D. R.; Wallace, G. G.; Officer, D. L., Steric Modification of a Cobalt Phthalocyanine/Graphene Catalyst To Give Enhanced and Stable Electrochemical CO_2 Reduction to CO. *ACS Energy Letters* **2019,** *4* (3), 666-672.
31. Wu, Y.; Hu, G.; Rooney, C. L.; Brudvig, G. W.; Wang, H., Heterogeneous Nature of Electrocatalytic CO/CO_2 Reduction by Cobalt Phthalocyanines. *Chemsuschem* **2020,** *13* (23), 6296-6299.
32. Zhang, X.; Wang, Y.; Gu, M.; Wang, M.; Zhang, Z.; Pan, W.; Jiang, Z.; Zheng, H.; Lucero, M.; Wang, H.; Sterbinsky, G. E.; Ma, Q.; Wang, Y.-G.; Feng, Z.; Li, J.; Dai, H.; Liang, Y., Molecular engineering of dispersed nickel phthalocyanines on carbon nanotubes for selective CO_2 reduction. *Nature Energy* **2020,** *5* (9), 684-692.

33. Kumar, A.; Prajapati, P. K.; Aathira, M. S.; Bansiwal, A.; Boukherroub, R.; Jain, S. L., Highly improved photoreduction of carbon dioxide to methanol using cobalt phthalocyanine grafted to graphitic carbon nitride as photocatalyst under visible light irradiation. *Journal of Colloid and Interface Science* **2019,** *543*, 201-213.
34. Do, K. H.; Praveen Kumar, D.; Putta Rangappa, A.; Wang, J.; Hong, Y.; Kim, E.; Amaranatha Reddy, D.; Kyu Kim, T., In situ preparation of polymeric cobalt phthalocyanine–decorated TiO_2 nanorods for efficient photocatalytic CO_2 reduction. *Materials Today Chemistry* **2021,** *22*, 100589.
35. Prajapati, P. K.; Singh, H.; Yadav, R.; Sinha, A. K.; Szunerits, S.; Boukherroub, R.; Jain, S. L., Core-shell Ni/NiO grafted cobalt (II) complex: An efficient inorganic nanocomposite for photocatalytic reduction of CO_2 under visible light irradiation. *Applied Surface Science* **2019,** *467-468*, 370-381.
36. Kumar, P.; Kumar, A.; Sreedhar, B.; Sain, B.; Ray, S. S.; Jain, S. L., Cobalt phthalocyanine immobilized on graphene oxide: an efficient visible-active catalyst for the photoreduction of carbon dioxide. *Chem. Eur. J* **2014,** *20*, 6154 – 6161.
37. Wang, J. W.; Jiang, L.; Huang, H. H.; Han, Z. J.; Ouyang, G. F., Rapid electron transfer via dynamic coordinative interaction boosts quantum efficiency for photocatalytic CO_2 reduction. *Nat Commun* **2021,** *12* (1), 4276.
38. Ma, B.; Chen, G.; Fave, C.; Chen, L.; Kuriki, R.; Maeda, K.; Ishitani, O.; Lau, T.-C.; Bonin, J.; Robert, M., Efficient Visible-Light-Driven CO_2 Reduction by a Cobalt Molecular Catalyst Covalently Linked to Mesoporous Carbon Nitride. *Journal of the American Chemical Society* **2020,** *142* (13), 6188-6195.
39. Li, H.; Xu, W.; Qian, J.; Li, T.-T., Construction of Polymeric Cobalt Phthalocyanine@ Mesoporous Graphitic Carbon Nitride Composite for Efficient Photocatalytic CO_2 Reduction. *Chemical Communications* **2021,** *57*, 6987-6990.
40. Liu, Y.; McCrory, C. C. L., Modulating the mechanism of electrocatalytic CO_2 reduction by cobalt phthalocyanine through polymer coordination and encapsulation. *Nat Commun* **2019,** *10* (1), 1683.
41. Słota, R.; Dyrda, G., UV Photostability of Metal Phthalocyanines in Organic Solvents. *Inorg Chem* **2003,** *42* (18), 5743-5750.
42. Zimmerman, J. L.; Williams, R.; Khabashesku, V. N.; Margrave, J. L., Synthesis of Spherical Carbon Nitride Nanostructures. *Nano Lett* **2001,** *1* (12), 731-734.
43. Cheung, P. L.; Kapper, S. C.; Zeng, T.; Thompson, M. E.; Kubiak, C. P., Improving Photocatalysis for the Reduction of CO_2 through Non-covalent Supramolecular Assembly. *Journal of the American Chemical Society* **2019,** *141* (38), 14961-14965.
44. Zhou, M.; Wang, S.; Yang, P.; Huang, C.; Wang, X., Boron Carbon Nitride Semiconductors Decorated with CdS Nanoparticles for Photocatalytic Reduction of CO_2. *ACS Catalysis* **2018,** *8* (6), 4928-4936.
45. Zhao, G.; Pang, H.; Liu, G.; Li, P.; Liu, H.; Zhang, H.; Shi, L.; Ye, J., Co-porphyrin/carbon nitride hybrids for improved photocatalytic CO_2 reduction under visible light. *Applied Catalysis B: Environmental* **2017,** *200*, 141-149.
46. Li, X.; Song, X.; Ma, C.; Cheng, Y.; Shen, D.; Zhang, S.; Liu, W.; Huo, P.; Wang, H., Direct Z-Scheme WO3/Graphitic Carbon Nitride Nanocomposites for the Photoreduction of CO_2. *Acs Appl Nano Mater* **2020,** *3* (2), 1298-1306.
47. Shi, L.; Wang, T.; Zhang, H.; Chang, K.; Ye, J., Electrostatic Self-Assembly of Nanosized Carbon Nitride Nanosheet onto a Zirconium Metal–Organic Framework for Enhanced Photocatalytic CO_2 Reduction. *Adv Funct Mater* **2015,** *25* (33), 5360-5367.
48. Zhou, M.; Wang, S.; Yang, P.; Luo, Z.; Yuan, R.; Asiri, A. M.; Wakeel, M.; Wang, X., Layered Heterostructures of Ultrathin Polymeric Carbon Nitride and $ZnIn_2S_4$ Nanosheets for Photocatalytic CO_2 Reduction. *Chemistry – A European Journal* **2018,** *24* (69), 18529-18534.
49. Mo, Z.; Zhu, X.; Jiang, Z.; Song, Y.; Liu, D.; Li, H.; Yang, X.; She, Y.; Lei, Y.; Yuan, S.; Li, H.; Song, L.; Yan, Q.; Xu, H., Porous nitrogen-rich g-C_3N_4 nanotubes for efficient photocatalytic CO_2 reduction. *Applied Catalysis B: Environmental* **2019,** *256*, 117854.

50. Ji, S.; Qu, Y.; Wang, T.; Chen, Y.; Wang, G.; Li, X.; Dong, J.; Chen, Q.; Zhang, W.; Zhang, Z.; Liang, S.; Yu, R.; Wang, Y.; Wang, D.; Li, Y., Rare-Earth Single Erbium Atoms for Enhanced Photocatalytic CO_2 Reduction. *Angewandte Chemie International Edition* **2020,** *59* (26), 10651-10657.
51. Chen, P.; Lei, B.; Dong, X. a.; Wang, H.; Sheng, J.; Cui, W.; Li, J.; Sun, Y.; Wang, Z.; Dong, F., Rare-Earth Single-Atom La–N Charge-Transfer Bridge on Carbon Nitride for Highly Efficient and Selective Photocatalytic CO_2 Reduction. *ACS Nano* **2020,** *14* (11), 15841-15852.
52. Ahn, H. S.; Yano, J.; Tilley, T. D., Photocatalytic water oxidation by very small cobalt domains on a silica surface. *Energy & Environmental Science* **2013,** *6* (10), 3080-3087.
53. Zhu, M.; Ye, R.; Jin, K.; Lazouski, N.; Manthiram, K., Elucidating the Reactivity and Mechanism of CO_2 Electroreduction at Highly Dispersed Cobalt Phthalocyanine. *ACS Energy Letters* **2018,** *3* (6), 1381-1386.
54. Pauly, M.; Kroger, J.; Duppel, V.; Murphey, C.; Cahoon, J.; Lotsch, B. V.; Maggard, P. A., Unveiling the Complex Configurational Landscape of the Intralayer Cavities in a Crystalline Carbon Nitride. *Chemical Science* **2022,** *13*, 3187-3193.
55. Kasap, H.; Caputo, C. A.; Martindale, B. C. M.; Godin, R.; Lau, V. W.-h.; Lotsch, B. V.; Durrant, J. R.; Reisner, E., Solar-Driven Reduction of Aqueous Protons Coupled to Selective Alcohol Oxidation with a Carbon Nitride–Molecular Ni Catalyst System. *Journal of the American Chemical Society* **2016,** *138* (29), 9183-9192.
56. Godin, R.; Wang, Y.; Zwijnenburg, M. A.; Tang, J.; Durrant, J. R., Time-Resolved Spectroscopic Investigation of Charge Trapping in Carbon Nitrides Photocatalysts for Hydrogen Generation. *Journal of the American Chemical Society* **2017,** *139* (14), 5216-5224.

TOC

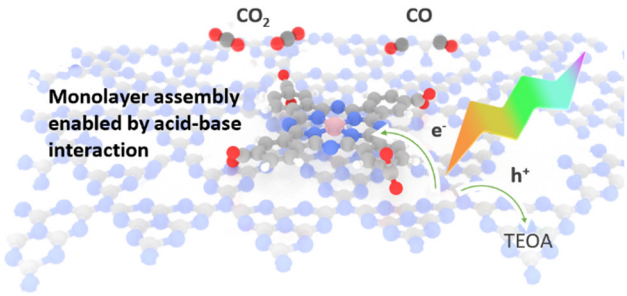
CO2
CO
Monolayer assembly
enabled by acid-base
interaction
e-
h+
TEOA